PHYSICAL REVIEW B VOLUME 27, NUMBER 8 15 APRIL 1983

Electronic structure of substitutional chalcogen impurities in silicon

Vijay A. Singh*
Solar Energy Research Institute, Golden, Colorado 80401

U. Lindefelt
Department of Theoretical Physics, University of Lund, Sölegatan 14A, S-233 62 Lund, Sweden

Alex Zunger
Solar Energy Research Institute, Golden, Colorado 80401
and Department of Physics, University of Colorado, Boulder, Colorado 80309
(Received 15 November 1982)

We report the results of a first-principles calculation of the electronic structure of substitutional, unrelaxed, and neutral chalcogen impurities (O, S, and Se) in silicon. We have employed the recently developed quasi band crystal-field defect Green's-function method. We find that whereas atomistic models predict that the binding energies of donor levels in semiconductors increase with the ionization potential of the free impurity atoms, a special enhancement of the screening in the solid predicts, for chalcogen impurities in silicon, a reversal in this order. Our results are in excellent agreement with recently reported optical excitation data available for Si:S and Si:Se. We demonstrate that whereas oxygen shows the expected *sp* bonding to the host crystal, sulfur and selenium exhibit also significant *d* bonding by utilizing their virtual *d* states. We discuss the relevance of effective-mass—type calculations to chalcogen impurities in the light of our results.

I. INTRODUCTION

The group-VI*A* (chalcogen) impurities in silicon have been the subject of intense investigation over the past two decades. The problems encountered in their study are interesting from both a purely scientific as well as a technological viewpoint.

Oxygen is the commonest contaminant in crucible-grown silicon and has hence been the subject of considerable work (e.g., see Refs. 1—3 for recent reviews). One reason is the advent of very-large-scale integration (VLSI) technology where one needs ultrapure silicon in order to produce VLSI chips for digital electronic devices.[2,3] Experimentally, Si:O was the subject of a pioneering study by Watkins and Corbett[4] (the "*A* center"). Their EPR work identified it as a defect located off the substitutional site. Sulfur is experimentally the best-studied deep impurity in silicon (see review of literature in Ref. 5). This is probably because one of the commonest centers concerning sulfur ("sulfur II,"[6] see below) is believed to be an ideal substitutional defect in silicon. The chalcogen defects in silicon are potential materials for thermal imaging and infrared-detection work.[7,8] It is believed that it could supersede and replace indium in this role. Selenium has been the subject of recent, very interesting optical excitation studies.[9,10]

Like other chemically reactive impurity elements, the chalcogens can form molecular complexes with the host semiconductor as well as with native and with intentionally introduced impurities. However, the chemical identity of such complexes remains largely unknown. It has therefore been difficult to associate experimental observations on chalcogen-containing semiconductors [e.g., EPR, deep-level transient spectroscopy (DLTS), and infrared-absorption data] with well-characterized chemical species. Our aim is to perform the first systematic self-consistent theoretical study on a series of chalcogen impurities in silicon in the simplest configuration—undistorted substitutional impurities—and establish the expected chemical trends in the electronic properties along this series.

Table I summarizes some pertinent data on chalcogen atoms that can be used to form an *a priori* intuition on the chemical trends. It includes the calculated[11] (using unrelativistic restricted Hartree-Fock formalism in the Koopmans limit) and measured[12] differences ΔE_s and ΔE_p in *s* and *p* valence orbital ionization energies between the chalcogen atom and Si, the differences in the Bragg-Slater[13] atomic radii (ΔR^{BS}) and Pauling's tetrahedral radii[14] (ΔR^T), as well as the differences in Sanderson's[15] and

 ©1983 The American Physical Society

TABLE I. Summary of data pertaining to some chemical trends in the chalcogen elements. ΔE_s and ΔE_p are the differences between the chalcogen and Si valence ionization energies for s and p orbitals, respectively. We give both calculated results [restricted nonrelativistic Hartree-Fock formalism in the Koopmans limit (Ref. 11)] and measured results (Ref. 12). $\Delta R^{\rm BS}$ and ΔR^{T} are the differences in the Bragg-Slater (BS, Ref. 13) and Pauling's (Ref. 14) tetrahedral (T) radii of the chalcogen element and Si. $\Delta\chi^{S}$ and $\Delta\chi^{P}$ are the corresponding differences in the Sanderson (S, Ref. 15) and Pauling (P, Ref. 16) electronegativities.

Quantity	O	S	Se	Te
$\Delta E_s^{\rm calc}$ (eV)	19.1	9.2	8.1	4.4
$\Delta E_p^{\rm calc}$ (eV)	9.1	3.8	2.9	1.7
$\Delta E_s^{\rm expt}$ (eV)	15.0	6.7	6.7	4.4
$\Delta E_p^{\rm expt}$ (eV)	5.5	2.3	1.6	0.9
$\Delta R^{\rm BS}$ (Å)	−0.5	−0.10	0.05	0.30
ΔR^{T} (Å)	−0.5	−0.13	−0.03	0.15
$\Delta\chi^{S}$	2.37	1.28	1.37	0.75
$\Delta\chi^{P}$	1.7	0.7	0.6	0.3

Pauling's[16] atomic electronegativities $\Delta\chi^{S}$ and $\Delta\chi^{P}$, respectively. Except for $\Delta\chi^{S}$, all the data are monotonic along the chalcogen series: Going down column VI*A* of the Periodic Table, the propensities of these elements to bind their atomic valence electrons decreases and their size increases. This is consistent[17] with the trends in the solubilities of chalcogen impurities in silicon.[18] Note, however, that the observed s-orbital binding energies of S and Se are closer than the calculated ones, and that concomitantly $\Delta\chi^{S}$ (in contrast to $\Delta\chi^{P}$) shows Se to be somewhat more electronegative than S. Our objective will be to establish the extent to which the chemical trends apparent from atomic physics and chemical scales (Table I) carry over to the condensed phase.

We have employed the recently developed quasi band crystal-field (QBCF) defect Green's-function technique[19] to study the electronic structure of O, S, and Se in silicon (Te is not included due to the predominance of relativistic effects[5]). Details of the technique have been published elsewhere.[19] We shall not describe them in this paper except to characterize the computational input to the present calculation. The calculations are performed within the framework of local-density-functional formalism. First-principles nonlocal pseudopotentials are employed.[20] The calculations were carried through to self-consistency of better than 10 mRy in the potential. The defect had a neutral configuration and was situated at the substitutional site, and no relaxation was considered. The spectral expansion of the defect wave functions in terms of host (plane-wave-based) Bloch wave functions consisted of an average of 30 bands for each $\vec{k}$ point, plus four quasi bands.[19] These were constructed from a linear combination of the exact (numerical) local-density valence pseudo-orbitals of the impurity atoms. The local representation of the defect wave functions consisted of 12 s, 11 p, 11 d, 10 f, and 10 g quantum-defect orbitals[21] (i.e., solutions of a radial atomiclike potential $b/r^2-a/r$) with optimized parameters $a=12.5$ a.u.$^{-1}$ and $b=1.0$ a.u.$^{-2}$. Counting both radial and angular components, this single-center basis consisted of 12 s, 33 p, 55 d, 70 f, and 90 g orbitals, or a total of 260 local orbitals. This set was augmented by the numerical s and p valence pseudo-orbitals of the impurity atom, calculated from an integration of the atomic Schrödinger equations. Potential perturbations and differences in charge densities were expanded in Kubic harmonics up to an angular momentum of 8. The electronic structure of the host crystal was obtained from a self-consistent pseudopotential band structure, using an exchange coefficient $\alpha=1$, as described previously.[22] Such a large exchange coefficient is needed in a local screening calculation to produce a physically correct band gap[19,22] (1.2 eV in the present study). Detailed convergence studies were carried out as before[19] to assure a precision of $\sim$0.1 eV in energies and $\sim$2% in charge densities.

In Sec. II we briefly recapitulate recent experimental work on these impurities, which may have a direct bearing on our calculations. In Sec. III we predict the location of impurity levels, the form of the impurity wave functions, and the values of the impurity charge densities. We compare our predictions with previously reported theoretical calculations and with experiment, wherever possible. In Sec. IV we discuss the chemical trends in the calculated impurity gap levels and compare them with what can be expected from atomic physics and chemical scaling arguments (Table I). We find an interesting reversal in the order of the levels in the solid relative to their order in free atoms. This points to the importance of self-consistent screening effects in the solid, discussed in Sec. IV. In Sec. V we compare our results for Si:Se with optical excitation studies that have recently been performed. We give corresponding values for the case of Si:S. In Sec. VI we discuss briefly the validity of previous calculations based on effective-mass theory in the light of our calculations.

II. THE EXPERIMENTAL SITUATION

We briefly review the present status of the experimental situation. The experimental literature is enormous, and we shall limit ourselves to discussing some recent work that has a direct bearing on our

calculations.

According to the recent work of Brotherton *et al.*,[6] there are three categories of sulfur level in silicon, termed S I, S II, and S III. Measuring energies with respect to the minimum of the conduction band E_c, the S I levels occur in a pair at $E_c-0.18$ eV (*A* level) and $E_c-0.38$ eV (*B* level). These S I levels appear in high concentration after high-temperature diffusion at 1200 °C. The S II levels also occur in a pair: the *C* level and *D* level. They appear in high concentration with low-temperature diffusion or slow cooling. The energy of the *C* level is $E_c-0.32$ eV if it is deduced from an $\ln(e_n^t)$ vs $1/T$ plot, and the temperature dependence of the capture cross section is taken into account.[6] The energy of the *D* level measured[5,23] in the same fashion is $E_c-0.59$ eV; however, when it is deduced from a $\ln(e_n^t/T^2)$ vs $1/T$ plot,[6] the result is $E_c-0.53$ eV. Processing the data of Ref. 6 by the former method gives $E_c-0.59$ eV. The most reliable value comes from optical measurements and gives $E_c-0.613$ eV. There is one S III level at $E_c-0.08$ eV. Brotherton *et al.* performed Hall-effect and diode *C-V* measurements (including DLTS) to determine the above-mentioned levels. They reviewed most of the previously reported levels and were able to fit them into the above three categories. In a parallel work, Grimmeiss and co-workers[5,23–25] performed extensive and very careful optical and electrical measurements on the S II center (*C* and *D* levels). The terminology used by Grimmeiss *et al.* is different (they refer to the *C*,*D* levels as *B*,*A* centers, respectively). We shall follow the notation of Brotherton *et al.*[6] in order to avoid confusion. Both groups agree on the values obtained for S II up to a few milli-electron-volts (meV). There is some discrepancy about the other centers S II and S III. In a recent photoconductivity study, Humphreys *et al.*[26] provided a very accurate estimate of the S II (*C* level) as well as the experimental binding energy of the excited states of this level. All three works are in agreement over the value $E_c-0.32$ eV for the S II (*C* level). Furthermore, apart from a study by Myers and Phillips,[27] the concentration profiles and density of the *C* and *D* levels have been found to be equal by many workers.[5,6,23] Thus it is logical to conclude that the two levels *C* and *D* are two charge states of the same center. Reinforcing this is the fact that the capture cross section of level *D* at 300 K is greater than 6×10^3 times that of level *C* extrapolated to 300 K. Hence one may associate the *C* level with neutral sulfur S^0 (i.e., a $S^0\rightarrow S^+$ transition) and the *D* level with a positively charged S^+ (i.e., $S^{1+}\rightarrow S^{2+}$ transition). The concept of sulfur as double donor would imply that the *D* level is paramagnetic, and in the EPR work this level has been identified as having tetrahedral symmetry.[28,29] The *C* level has not been detected in EPR studies. This may be indicative of a closed-shell a_1^2 configuration of S^0. The above arguments form the basis of the widely held opinion that the S II (*C* level) is a neutral, substitutional, unrelaxed impurity in silicon. For the sake of completeness, we shall mention that the S I levels are believed to be[6] charge states of S-impurity pairs, and the S III is believed to be a complex of S and a dopant impurity.

Comparable studies have recently been done[5] for Se and Si in which the counterpart of S II levels were identified. For Se, these are at $E_c-0.30$ eV (*C* level) and $E_c-0.52$ eV (*D* level, from e_n^t vs $1/T$ plots without correction for the temperature dependence of the cross section) or $E_c-0.59$ eV (from optical data,[5(b)] cf. Refs. 23, 25, and 30). Furthermore, very interesting infrared-absorption studies have recently been performed to determine the excited-state ladder of the $E_c-0.30$ eV center.[9,10] In one of them,[10] similar results were reported for mass-transported and diffused Se. It is with these infrared-absorption studies that we will compare our calculations in Sec. V.

An enormous amount of data exists for O in Si. There is no indication that O forms a simple defect in Si. A discussion of oxygen levels invariably involves consideration of complexes[1,4,31,32]: SiO_4, SiO_5, vacancy-oxygen pairs, etc. Oxygen behaves very differently from S and Se. In our calculation we shall look for departures from established chemical and atomic trends. This could provide some insight into the anomalous behavior of oxygen.

We note that simple chemical considerations already point to the possibility that whereas O will not form simple substitutional impurity in Si (i.e., tetrahedral bonding), S and Se will. The large atomic size and electronegatively mismatch between O and Si compared with the smaller differences for S and Se (Table I) point to this direction. Furthermore, S and Se do form stable molecules with Si where the Si—S—Si or the Si—Se—Si bond angles are close to tetrahedral. For example, tetramethyl cyclodisilthiane and hexamethyl cyclotrisilthiane[33] have bond angles Si—S—Si of 110°. Also, the compounds SiS_2 and $SiSe_2$ show at high pressure a cristobalitelike (SiO_2) structure in which the bond angle around the chalcogen is close to tetrahedral, in contrast to the values of 140°–150° in SiO_2.[34] Tetrahedral bonding of oxygen with relatively electropositive elements like Si are virtually unknown.

III. RESULTS

Figure 1 depicts the deep defect-induced electronic levels for O, S, and Se as obtained by our calcula-

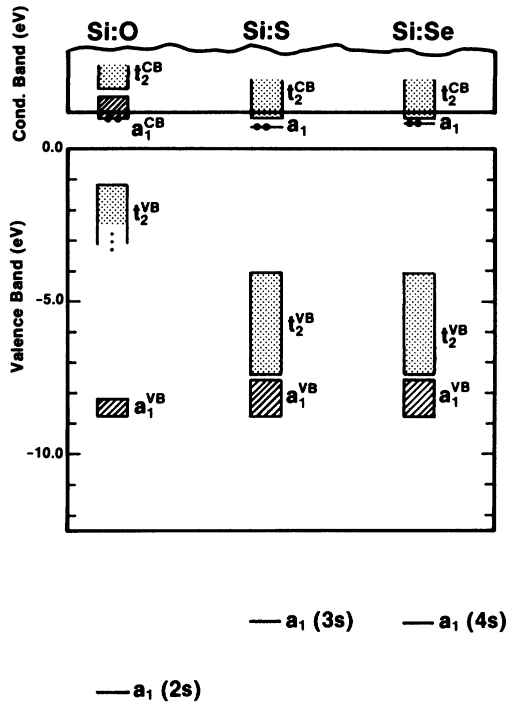

FIG. 1. Schematic view of the calculated deep impurity levels of neutral, substitutional O, S, and Se in Si. Resonances are shown as shaded (t_2) or cross-hatched (a_1) areas. The demarcation line for resonances is approximate. Gap levels are shown as solid lines, where the occupation is denoted by solid circles. (The shallow e and t_2 states in the gap, not shown on the scale of this figure, are depicted on an enlarged scale in Fig. 8.)

tion. The discussion of the shallow e and t_2 levels (cf. Fig. 8, not shown on the scale of Fig. 1) will be deferred to Sec. V. We shall first discuss the levels of a_1 symmetry and next those of t_2 symmetry.

An inspection of Fig. 1 shows that levels of a_1 symmetry may be divided into two groups. In the first group we have a hyperdeep a_1 level below the valence-band minimum and a broad resonance a_1^{VB} around $E_{VBM}-8$ eV, where VBM is the valence-band maximum. They may be viewed as the bonding and antibonding configurations of the impurity-atom valence s levels and the vacancy a_1 resonance[19] at $\simeq E_{VBM}-8.0$ eV. Figure 2 depicts for Si:S the angular momentum components[19] $G_l^{a_1}(|\vec{r}|)$ of these wave functions. The hyperdeep level [Fig. 2(a)] is seen to be nodeless, confined in the central cell and almost exclusively s-like. In fact, it is very similar to the outer valence s pseudo-orbital of the free impurity atom. In contrast, the a_1^{VB} resonance [Fig. 2(b), depicting a level at $E_{VBM}-8.2$ eV from this resonance] is seen to have a node in the central cell and to be a s-f hybride.

The second group of a_1 impurity levels lies above the valence-band maximum (Fig. 1). S and Se have a_1 levels deep in the gap and are doubly occupied. The radial components of this wave function are depicted in Fig. 2(c) for Si:S. It is seen to have a node halfway between the impurity and its nearest neighbor, and to be predominantly s-like. Table II gives[35–39] the energy values obtained by our calculations and compares them with other calculations. Table III provides information on the degree of localization of the defect-induced wave functions. It

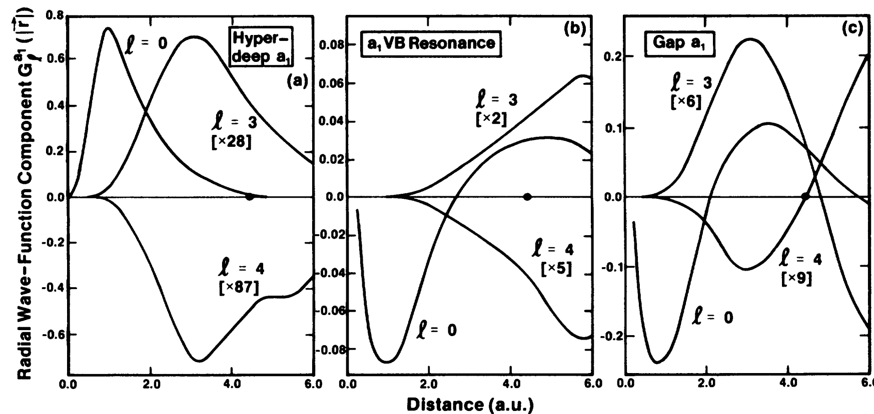

FIG. 2. Radial components of the defect-induced a_1 wave functions of Si:S. (a) hyperdeep a_1, (b) a_1 valence-band resonance, (c) a_1 gap orbital. The solid circle indicates the position of the nearest-neighbor Si atom.

TABLE II. Summary of calculated gap levels of a_1 symmetry for substitutional Si:O, Si:S, and Si:Se. The numbers represent distance from the conduction-band edge. All values are in eV. We show the results of the present work both as orbital energies and as removal energies (transition-state values) that can be compared with experiment. For comparison, the observed values for the *C* center are given. The values from Ref. 36 are interpolated graphically.

Workers	O	S	Se
Fletcher (Ref. 35)	0.26	0.17	0.16
Hjalmarson *et al.* (Ref. 36)	~1.2	~0.6	~0.5
Pantelides and Sah (Ref. 37)		0.33	0.36
Pantelides (Ref. 38)		0.41	0.27
Bernholc *et al.* (Ref. 39)		0.10	
Present Work			
Orbital energies	0.06	0.29	0.26
Removal energies		0.32	0.29
Expt. [*C* center, Refs. 5(a) and 5(b)]		0.318	0.306

depicts the percentage of electronic charge enclosed in a sphere of radius R around the impurity site for both the gap and the hyperdeep a_1 levels. It shows that whereas the hyperdeep a_1 level is extremely localized, its counterpart in the gap has only a quarter of its charge in the central cell. The partial wave analysis of Table IV indicates that most of the charge in the a_1 gap levels is *s*-like, with only a small admixture of *f* character.

The pioneering work of Fletcher[35] is based on an empirically parametrized Koster-Slater approach to the defect Green's function. Hjalmarson *et al.*[36] employed a similar tight-binding approach. In both calculations the defect energy levels are determined by the choice of the diagonal perturbation parameters ΔE_s (Table I), since no off-center coupling with the host crystal was allowed. A great amount of the variations in the predicted positions of these gap levels (e.g., $E_c-0.26$, $E_c-0.17$, and $E_c-0.16$ eV for O, S, and Se in Ref. 35, compared with $E_c-1.2$, $E_c-0.6$, and $E_c-0.5$ eV in Ref. 36) is associated with different choices of the atomic input ΔE_s (in Ref. 36 the $\Delta E_s^{\rm calc}$ values of Table I were used, which differ from the observed $\Delta E_s^{\rm expt}$ values; cf. S and Se).

The results of Table II show a considerable spread in the predicted a_1 gap level energies, highlighting the difficulties in such calculations. In fact, different authors compared their predicted results with different observed values (centers *A*—*D* in Sec. II). For example, for the case of S the work of Fletcher[35] is closer to S I (*A* level[6]), and the work of Hjalmarson[36] is closer to S II (*D* level[6]), as opposed to being closer to S II (*C* level[6]). Both of these calculations as well as ours suggest the same trend: S is slightly deeper than Se. This trend parallels the trend in ΔE_s and is consistent with a wide body of experimental data that finds the Se energies to be 10% smaller than those of S.[30] [Note, however, that the fact that tight binding predicts S to be deeper than Se is at least partially an artifact of the choice of Hartree-Fock energy parameters $\Delta E_s^{\rm calc}(\text{S}) > \Delta E_s^{\rm calc}(\text{Se})$, as opposed to the experimental values $\Delta E_s^{\rm expt}(\text{S}) = \Delta E_s^{\rm expt}(\text{Se})$.] In all our calculations, in-

TABLE III. Percentage of the normalized electronic charge enclosed within a sphere of radius R around the impurity site, for the gap and hyperdeep levels, both of a_1 symmetry. Nearest-neighbor distance is denoted by d (4.44 a.u.). The next-nearest neighbor is at $1.63d$.

Impurity	Level	$R=d/2$	$R=d$	$R=1.63d$
O	Gap	1%	9%	16%
S	Gap	6%	29%	47%
Se	Gap	6%	27%	45%
O	Hyperdeep	94%	100%	100%
S	Hyperdeep	70%	97%	100%
Se	Hyperdeep	66%	96%	100%

TABLE IV. Energies, orbital density localization parameters q^{α} and their angular momentum components q_l^{α} of the a_1 gap level, one of the t_2 resonance levels in the valence band, and one in the conduction band. E_c and E_{VBM} represent the bottom of the conduction band and the top of the valence band, respectively. The q^{α} represents the electronic charge enclosed in a sphere of radius 4.44 a.u. (nearest-neighbor distance) around the impurity site, normalized to 1.0. The a_1 states are doubly occupied, the conduction-band t_2 states are empty, and the valence-band t_2 states are sixfold occupied. q_l^{α} represents its decomposition into angular momentum components (Ref. 22).

Impurity	State	e (eV)	Symmetry	q_s^{α}	q_p^{α}	q_d^{α}	q_f^{α}	$q^{\alpha}(e)$
O	Gap states	$E_c-0.06$	a_1	92%	0	0	7%	0.088
S		$E_c-0.29$	a_1	92%	0	0	8.1%	0.29
Se		$E_c-0.26$	a_1	92%	0	0	5%	0.27
O	t_2^{VB} resonance	$E_{\text{VBM}}-1.79$	t_2	0	97%	2.0%	$<1\%$	0.22
S		$E_{\text{VBM}}-5.14$	t_2	0	98%	1.2%	$<1\%$	0.21
Se		$E_{\text{VBM}}-5.13$	t_2	0	98%	1.5%	$<1\%$	0.19
O	t_2^{CB} resonance	$E_{\text{VBM}}+2.00$	t_2	0	66%	32%	$<1\%$	0.10
S		$E_{\text{VBM}}+1.58$	t_2	0	23%	75%	$<1\%$	0.11
Se		$E_{\text{VBM}}+1.59$	t_2	0	20%	78%	$<1\%$	0.11

cluding the transition-state calculations (labeled "removal energy" in Table II) which we shall discuss in Sec. IV, we find that the Se gap energies are 5–10% smaller than those for S. (Although our calculations are accurate to a tenth of an electron volt, we have displayed numbers to a hundreth of an electron volt in order to emphasize this reproducible difference between Se and S and hence the suggested trend.)

A self-consistent Green's-function calculation similar in spirit to ours (but using an empirical local pseudopotential) has been performed for Si:S by Bernholc *et al.*[39] They report a gap level of a_1 symmetry 0.1 eV below the conduction-band edge compared with 0.29 eV obtained by us. Overall, the best agreement with experiment is obtained by the QBCF result of the present work (Table II).

The calculations in Refs. 37, 38, and 40 for Si:S and Si:Se are based on an extension of effective-mass theory (EMT) to double donors. The analogy in this is with the helium atom as opposed to the hydrogen atom.[41] Table II shows that the EMT calculations based on pseudopotentials[37] yields Se to be deeper than S in opposition to all other calculations. The EMT calculations based on the point-charge model[38] show a substantial difference between Se and S, and this is again in contradiction with other calculations as well as with experimental observation.[6,30] Other EMT calculations have been reviewed by Pantelides.[42]

All calculations for Si:O summarized in Table II pertain to a substitutional unrelaxed geometry. The predicted binding energies cannot be compared with experiments (a value of $E_c-0.17$ eV has been proposed[4]) that pertain to a strongly relaxed configuration.

The oxygen a_1 gap level, like those for neutral S and Se, is also doubly occupied. However, it is much closer to the conduction-band edge as shown in Table II. This closeness results in resonance; the a_1 gap level for Si:O is a tail of a broad conduction-band resonance, peaking around $E_{\text{VBM}}+1.5$ eV. We note from Table II that our oxygen result is at odds with all previous calculations: It does not follow the monotonic trend with the ionization potential differences ΔE_s. We shall discuss this significant irregularity and its implications on the screening mechanism in the solid in the next section.

There exist several cluster calculations for chalcogens in silicon. In the multiple-scattering (MS) $X\alpha$ work of Cartling,[43] the transition-state calculation for the S a_1 gap state yields $E_c-0.39$ eV, close to the value of $E_c-0.32$ eV obtained here. In a simlar MS $X\alpha$ calculation, Caldes *et al.*[44] obtained for O an a_1 level in the middle of the gap. This level certainly appears to be deeper than S, similar to the findings of Refs. 35 and 36. Both MS $X\alpha$ calculations show a hyperdeep level for S and O, similar to ours. However, Table III shows that the a_1 gap level wave functions are very extended (in particular, for Si:O). In fact, they sample mainly the potential outside the second Si shell. Small-cluster calculations (including one[43] or two[44] Si shells) miss the significant interaction and may hence produce results for the gap levels that are less reliable (i.e., too deep relative to E_c) than those for the hyperdeep levels. This is highlighted by the fact that a QBCF calculation for Si:S in which one impurity is placed in a re-

TABLE V. Population analysis of the occupied states for the O, S, and Se in Si. See definitions in text and in Ref. 22.

Impurity	Angular momentum	$Q_l^{a_1}$	Q_l^e	$Q_l^{t_1}$	$Q_l^{t_2}$	Q_l
O	$l=0$	2.4260	0	0	0	2.4260
	$l=1$	0	0	0	7.5024	7.5024
	$l=2$	0	0.2575	0	0.8198	1.1073
	$l=3$	0.0934	0	0.3883	0.1399	0.6216
	$l=4$	0.0132	0.0800	0.0689	0.1777	0.3494
	Q^{α}	2.533	0.368	0.457	8.640	$Q^{\text{tot}}=12.00$
S	$l=0$	2.8498	0	0	0	2.8498
	$l=1$	0	0	0	6.1644	6.1644
	$l=2$	0	0.4362	0	1.0646	1.5008
	$l=3$	0.1562	0	0.5248	0.1809	0.8619
	$l=4$	0.0170	0.1002	0.0857	0.1895	0.3924
	Q^{α}	3.0230	0.5364	0.6110	7.5994	$Q^{\text{tot}}=11.77$
Se	$l=0$	2.8128	0	0	0	2.8128
	$l=1$	0	0	0	6.0450	6.0450
	$l=2$	0	0.4695	0	1.1468	1.6163
	$l=3$	0.1526	0	0.5431	0.1897	0.8854
	$l=4$	0.0165	0.1809	0.0877	0.1809	0.3870
	Q^{α}	2.9819	0.5714	0.6008	7.4624	$Q^{\text{tot}}=11.75$

only its valence *sp* orbitals. Indeed, the chemistry of S compounds[45] suggests the decisive role of *d* hybridization (e.g., the near linearity of the H_2S molecule, impossible within the *sp*-bonding picture, as opposed to the 105° bond angle in H_2O). We note that the pronounced non-*sp* character of the central cell charge for Si:S and Si:Se cannot be faithfully revealed by tight-binding models[35,36] (which restrict the basis set to *sp* orbitals only; hence only off-center *d* character is allowed), or by local pseudopotential models[39] (which force the *d* part of the wave functions to sample the same potential that the *sp* piece "feels"; hence *d* states are artificially pushed to higher energies). Table V also shows that the *e* and t_1 character of the system is relatively small and fairly constant along the series, consistent with the fact that there are no strongly localized defect-induced *e* and t_1 resonances in the system (the shallow *e* level is extended and effective-mass-like; cf. Sec. V). Finally, if one subtracts from the Q_l values of Table V the corresponding values for the Si vacancy,[19] one finds that the effective configuration of substitutional oxygen in silicon is closer to s^1p^5 (*sp* bonding) than to its free-atom configuration s^2p^4 (*p* bonding).

IV. REVERSAL OF ORDER OF DEFECT LEVELS WITH ATOMIC IONIZATION ENERGIES

In this section we discuss the calculated chemical trends in the binding energies of the a_1 gap levels, in light of intuitive chemical models advanced on the basis of the data of Table I. The basic phenomena is that the order of the a_1 binding energy that we find ($E_c-0.06$, $E_c-0.29$, and $E_c-0.26$ eV for Si:O, Si:S, and Si:Se, respectively; cf. Table II) shows a reversal in order relative to the atomic energy differences for the *s* orbitals ($\Delta E_s=15$, 6.7, and 6.7 eV for O, S, and Se, respectively; cf. Table I). This reversal persists when very accurate pseudopotentials are used (the trans-density-functional pseudopotentials of Ref. 20, which, among others, is norm conserving), when careful basis-set convergence studies are conducted, and when the asymptotic sum rule $[\lim_{r\to\infty}\Delta V(r)=2(Z_{\rm O}-Z_{\rm Si})=4]$ is strictly enforced. (The reversal may not occur if there is insufficient variational flexibility outside the central cell, where most of the amplitude of the gap wave function is concentrated.)

The underlying concept, used in defect theories as

peated supercell containing 250 atoms gives an a_1 gap level at $E_c - 0.47$ eV, whereas if the supercell is increased to include 1458 atoms, the level moves *up* to $E_c - 0.29$ eV.

We next discuss the levels of t_2 symmetry. There is a broadened t_2 resonance in the valence band (t_2^{VB} in Fig. 1) that has over 50% atomic character (i.e., in the expansion of the wave functions in local orbitals, the square of the coefficient of the free impurity-atom basis function exceeds 0.5). This is the counterpart of the a_1 hyperdeep level. This may be viewed as the bonding combination of the impurity p level with the vacancy[19] t_2 level. There is further a t_2 resonance in the conduction band, above the a_1 gap level (t_2^{CB} in Fig. 1). This is the continuation into the bands of a shallow and discrete t_2 level just below the conduction-band minimum (cf. Sec. V). Figure 3 depicts the wave functions of both the bonding valence-band t_2 resonance and for the antibonding conduction-band t_2 resonance, all plotted along the $\pm\langle 111\rangle$ crystal directions. The bonding t_2^{VB} resonance is nodeless in the central cell and p-type, whereas the antibonding t_2^{CB} resonance is a p-d hybride, has a node in the central cell, and is twice as delocalized in this region relative to the bonding t_2^{VB} resonance.

Table IV depicts the charge enclosed in a sphere of radius 4.44 a.u. (nearest-neighbor distance) by the a_1 gap and a t_2^{CB} resonance wave function. The t_2^{CB} conduction-band resonances have considerable $l=2$ character (i.e., they are p-d hybrids). [Tight-binding calculations[35,36] using only $l=1$ (p) orbitals may not be able to describe this adequately.] Note that the percentage of d character increases dramatically in going from Si:O to Si:S and Si:Se: The t_2 levels of the latter are predominantly d states. Table IV further shows that the a_1-t_2 splittings between the respective antibonding state (0.94,0.75,0.77 eV for O,S,Se, respectively, using the strongest t_2 conduction-band states shown in the table) follow the order expected from atomic physics for the s-p splittings Δ_{sp} in the free atoms [$\Delta_{sp}(\text{O}) \gg \Delta_{sp}(\text{Se}) \geq \Delta_{sp}(\text{S})$, cf. Table I].

Table V contains a population analysis of all the occupied valence states for O, S, and Se. Here (cf. Ref. 22) Q_l^{α} denotes the charge enclosed in a sphere of radius 4.44 a.u. for all states of representation $\alpha = a_1, e, t_1, t_2$ and angular momentum $l=0,1,2,3,4$. The orbital charge Q^{α} is $\sum_l Q_l^{\alpha}$ and hence shows the total charge in a given representation. Q_l is $\sum_{\alpha} Q_l^{\alpha}$ and represents the l character of all representations. Q^{tot} is $\sum_{\alpha} Q^{\alpha}$ and represents the total electronic charge in the central cell.

Table V shows that $Q_{l=0}$ is relatively small for O as compared to S and Se. This is due to the fact that the doubly occupied a_1 gap level for O is closer to the conduction band and more delocalized (cf. Table III). In contrast, the $Q_{l=1}$ and Q_{tot} of O is higher than S and Se. This implies that the perturbed valence band carries more charge in the central cell in the case of O. This is consistent with chemical electronegativity considerations. O is much more electronegative than S or Se and hence attracts more charge (cf. Table I). Note further that the non-sp character ($Q_{l=2}+Q_{l=3}+Q_{l=4}$) is considerably smaller for Si:O (2.0) than for Si:S (2.75) and Si:Se (2.9). This is consistent with the well-known[45] ability of S and Se to utilize their extravalence orbitals (e.g., $3d$ and $4d$ for S and Se, respectively) and form even sixfold-coordination compounds (e.g., SF_6), as opposed to the lower coordination possible for oxygen (e.g., OF_2), which utilized effectively

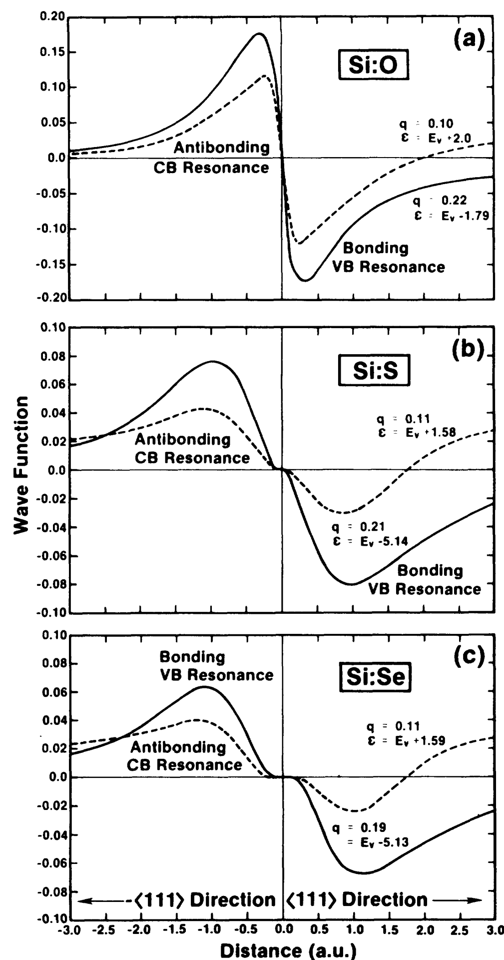

FIG. 3. t_2 bonding (solid lines) and t_2 antibonding (dashed lines) wave functions, plotted along the $\pm\langle 111\rangle$ crystal directions. (a) Si:O, (b) Si:S, (c) Si:Se.

diverse as effective-mass,[42] tight-binding,[35,36] and chemical scaling[46] approaches, has been that the binding energies E_b^I of different impurities I in the same host crystal are ordered according to the ionization potential differences $\Delta E(I-H)$ of the *isolated impurity atoms,* if one considers the same crystal-site location and charged state for all impurities. Various theoretical approaches have displayed the atomistic scaling hypothesis in different forms. They all predict a monotonic,[35,36] or near-monotonic,[37] variation of E_b^I with the defect-induced potential perturbation

$$\Delta V = V(\text{impurity}) - V(\text{host}) \ .$$

In turn, ΔV directly reflects in these theories the difference between the impurity (I) and host (H) *atomic* ionization potentials V_{IP}. For example,

$$\Delta V \propto V_{\text{IP}_I} - V_{\text{IP}_H} \equiv \Delta E(I-H)$$

in tight-binding models,[35,36]

$$\Delta V \propto V_I^{\text{ps}}(\vec{q}) - V_H^{\text{ps}}(\vec{q})$$

(in momentum space) in central-cell-corrected effective-mass models[37] (where V_i^{ps} is the bare pseudopotential of the free ion, whose depth is proportional to V_{IP_i}), and

$$\Delta V \propto |\chi_I - \chi_H|^2$$

in chemical scaling models[46] (where χ_i is the atomic electronegativity, proportional to V_{IP_i}). The underlying premise in these approaches is that the balance that exists in an isolated atom between the bare potential V^{ps} and the screening potential V^{scr} is inherently similar (or maintains a causal scaling relation) to that prevailing for an impurity atom bonded to a solid. We note, however, from Table III that the a_1 gap levels in silicon (antibonding combinations) are extended in coordinate space, in contrast to the far more compact valence s-orbital wave functions of the isolated impurity atoms. To what extent does this difference affect the ordering of the levels? A self-consistent approach to the problem offers the opportunity to explore this point. In this approach one specifies only the *external* bare perturbation associated with the impurity

$$\Delta V^{\text{ext}}(\vec{r}) = V^{\text{ps}}(\text{impurity}) - V^{\text{ps}}(\text{host}) \ , \qquad (1)$$

and asks what is the self-consistent screening perturbation

$$\Delta V^{\text{scr}}(\vec{r}) = V^{\text{scr}}(\text{impurity}) - V^{\text{scr}}(\text{host}) \qquad (2)$$

associated with it. The screening is calculated as a sum of the interelectronic Coulomb term $V_{ee}[\rho(\vec{r})]$ and the exchange-correlation term $V_{\text{xc}}[\rho(\vec{r})]$, both evaluated from the self-consistent electronic charge density

$$\rho(\vec{r}) = \sum_i^{\text{occ}} |\psi_i|^2$$

constructed from all occupied (occ) wave functions. We will therefore analyze the trends in energies in terms of the *screened* effective potential

$$\Delta V^{\text{eff}}(\vec{r}) = \Delta V^{\text{ext}}(\vec{r}) + \Delta V^{\text{scr}}(\vec{r}) \qquad (3)$$

and see to what extent it is dominated by the trends in the properties of the free atoms, expressed by $\Delta V^{\text{ext}}(\vec{r})$ alone. Note that non-self-consistent models assume that ΔV^{eff} is related to ΔV^{ext} by a simple, nearly constant factor. In tight-binding models the diagonal Hamiltonian element is taken as an impurity-independent constant times ΔE_s (the latter reflecting ΔV^{ext} alone), whereas in non-self-consistent effective-mass models one sets

$$\Delta V^{\text{eff}}(r) = \int_0^r [\Delta V_{\text{ext}}(q) e^{iqr} / \epsilon(q)] dq$$

[or even $\Delta V^{\text{eff}}(r) = \Delta V^{\text{ext}}(r)/\epsilon(r)$], and hence the trends in $\Delta V^{\text{eff}}(r)$ reflect primarily the trends in ΔV^{ext}, since $\epsilon(q)$ and $\epsilon(r)$ are related to the host alone.

Figure 4(a) displays the r-multiplied pseudopotential perturbation

$$r\,\Delta V^{\text{ext}}(r) \equiv r\,\Delta V_L^{\text{ps}}$$

for the s wave of Si:O, Si:S, and Si:Se. As expected from atomic considerations,[20] the O atom with its largest atomic s-orbital energy [$V_{\text{IP}} = 28.5$ eV (Ref. 12)] has the most attractive ΔV^{ps}, whereas Se with its smaller atomic-orbital s energy [$V_{\text{IP}} = 20.15$ eV (Ref. 12)] has the least attractive ΔV^{ps} [S is close to Se since its V_{IP} is 20.20 eV (Ref. 12)]. The upper panel in Fig. 4(a) shows for these impurities the spherical part ($l=0$) of the self-consistent screening perturbation $r\,\Delta V^{\text{scr}}(r)$. Both $r\,\Delta V^{\text{ps}}$ and $r\,\Delta V^{\text{scr}}$ attain their asymptotic limits of $-2\Delta Z$ and $2\Delta Z$, respectively, where $\Delta Z = 2$ is the difference in valence between the column-VI impurity and Si. The screening is seen to vary considerably from O to S and Se. The most electronegative element in the series (O) is seen to be capable of best attracting electronic charge to it, resulting in the most repulsive screening potential (cf. Table V for the total central-cell charges). In fact, oxygen in silicon is closer to an anion O^{-1} than to a neutral atom O^0. However, relative to the free atoms, the propensities for attracting charge to the impurity is considerably enhanced in the solid. This can be appreciated from Fig. 5. It displays the impurity-induced radial charge

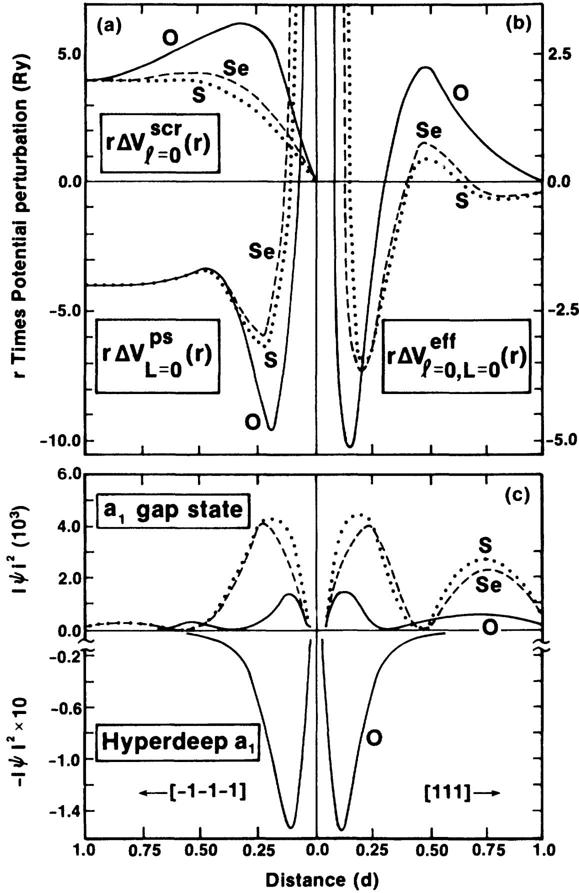

FIG. 4. (a) Spherical ($l=0$) screening ($r\,\Delta V^{scr}$) [Eq. (2)] and s pseudopotential ($r\,\Delta V^{ps}$) [Eq. (1)] perturbations. (b) Effective potential perturbation ($r\,\Delta V^{eff}$) [Eq. (3)]. (c) Orbital densities for the gap and hyperdeep a_1 defect wave functions. The impurities (O,S,Se) are substitutional, neutral, and unrelaxed in Si.

$$Q_{solid}(R)=\int_0^R [\rho_{Si:I}(\vec{r})-\rho_{Si}(\vec{r})]d\vec{r}$$

in a sphere of radius R around the impurity, as well as the analogous quantity for the free atoms

$$Q_{atoms}(R)=\int_0^R [n_I(\vec{r})-n_H(\vec{r})]d\vec{r}\ ,$$

where $n_i(\vec{r})$ are the free-atom pseudo-charge-densities. The charge densities of the impurity-containing solid ($\rho_{Si:I}$) and pure host crystal (ρ_{Si}) are calculated independently in a self-consistent fashion. The difference between $Q_{solid}(R)$ and $Q_{atoms}(R)$ is denoted in Fig. 5 as a shaded area and represents the excess charge around the impurity in the solid. Whereas the excess charge in *atomic* O and S (relative to Si) is seen to already exceed at $r \gtrsim 2$ a.u. its asymptotic value $\Delta Z=2$, when placed in the solid, O attracts significantly more charge than S relative to their atomic states. It is this screening enhancement that produces the most repulsive ΔV^{scr} in Si:O.

Figure 4(b) displays the spherical part of the s-wave effective potentials $r\,\Delta V^{eff}(r)$ for the three impurities. It is seen to delineate the space around the impurity into two regions with different properties. In the inner central cell (region I; $r \lesssim 0.25d$), ΔV^{eff} is dominated by ΔV^{ps} and hence maintains the atomic order $\Delta V^{eff}_{O} < \Delta V^{eff}_{Se}$. In the outer central cell (region II; $r \gtrsim 0.3d$), ΔV^{scr} dominates ΔV^{eff}, and the order is reversed to $\Delta V^{eff}_{O} > \Delta V^{eff}_{Se} \gtrsim \Delta V^{eff}_{S}$. Clearly, localized impurity states whose wave functions sample predominantly region I are likely to have a reversed order of binding energies relative to impurities with extended wave functions that are affected predominantly by the potential in region II. As we will shortly see, this is the case for the orbitals of the deep and hyperdeep levels, respectively.

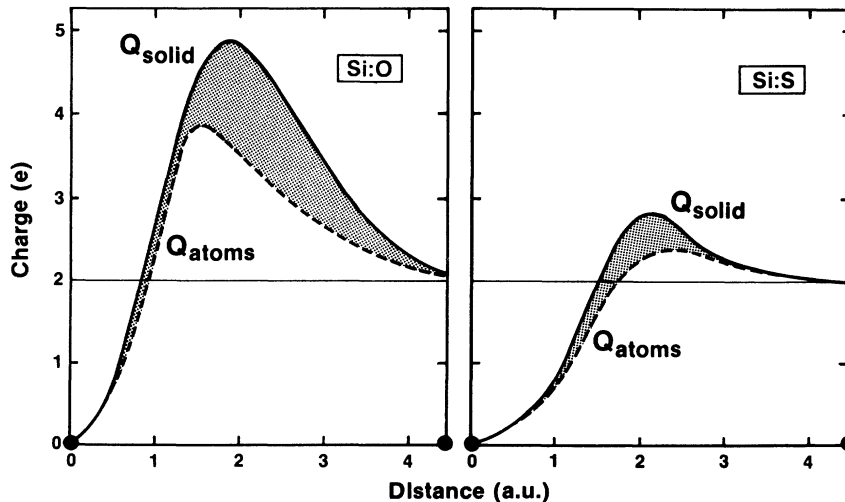

FIG. 5. Charge relative to Si enclosed in a sphere of radius R for O and S as impurities (Q_{solid}) and free atoms (Q_{atoms}). The shaded area denotes the excess charge in a solid.

Figure 4(c) shows for chalcogen impurities in Si the square of the hyperdeep and the gap a_1 wave functions along the $\pm\langle 111 \rangle$ crystal directions. The wave functions of the hyperdeep states are found to be nearly identical to those of the atomic *ns* state; the same order of orbital energies is found. These wave functions are localized almost entirely in region I (cf. Table III). On the other hand, the antibonding a_1 gap states have most of their amplitude in region II and beyond: The fact that the "impurity sphere" (orbital density of hyperdeep levels) and "impurity doughnut" (orbital density of gap levels) states occupy nearly mutually exclusive parts of space suggests that they will respond to the different ordering of the effective potentials in regions I and II. Figure 6 shows, on an expanded scale, the energies of the antibonding a_1 (doubly occupied) and t_2^{CB} (empty) levels of chalcogen impurities in Si. The a_1 gap level of O has the smallest one-electron binding energy (relative to the conduction-band minimum): $E_c - 0.06$ eV; it extends into the conductive band as a resonance. The one-electron binding energies of Se and S are $E_c - 0.26$ and $E_c - 0.29$ eV, respectively. Hence the most electronegative (or highest IP) element in the series has the smallest binding energy. Clearly, the use of atomic energies to replace self-consistent solid-state matrix elements, as done in defect tight-binding models,[35,36] is not generally valid.

We note that while the a_1-level reversal is predominantly a solid-state effect (cf. Fig. 5), it is already signaled by the properties of the atoms. In Fig. 7 we plot the atomic counterpart of the O and S solid-state potential perturbations shown in Fig. 4. The pseudopotentials are identical in both Figs. 4(a) and 7(b). It appears that the repulsive character of the atomic screening perturbation carries over into the solid. Thus the resulting repulsive screening of O is partly due to the remnant atomic property and largely due to electronegativity considerations that come into play when oxygen is inserted in the silicon matrix.

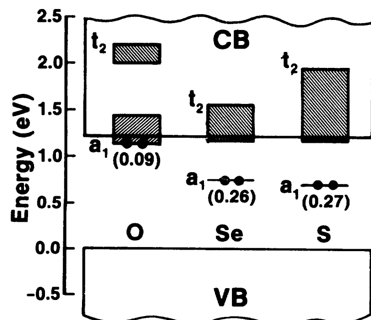

FIG. 6. Enlarged view of the spacings in a_1 and t_2 gap levels and resonances (shaded) for Si:O, Si:S, and Si:Se.

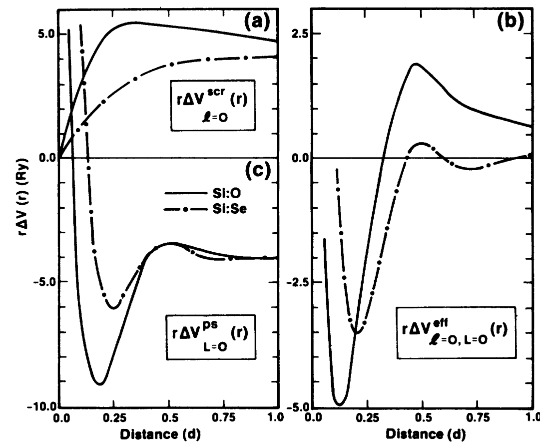

FIG. 7. Atomic counterpart of Figs. 4(a) and 4(b). Notation as in Fig. 4.

The reversal in the order of the a_1 gap levels has an important implication on the simple models used in the past to rationalize results for donor impurities. Numerous calculations on donor levels in semiconductors[36,39,47] have used a "defect-molecule model" to analyze the results of their calculations. In its simplest form, this model assumes that the interaction between the host vacancy a_1 level and the impurity *s* orbital creates a hyperdeep bonding level (often below the VB minimum) and a deep antibonding level at the vicinity of the band gap. (In a somewhat more complex model, the vacancy a_1 resonance at $E_{\mathrm{VBM}} - 8$ eV is also invoked.) The bonding level is constructed predominantly from the impurity atomic orbitals, whereas the antibonding level is constructed primarily from the vacancy a_1 orbitals. There are two tacit consequences to this model: (i) Since the vacancy a_1 level is constructed primarily from valence-band states,[19,36,47] the model views the antibonding donor a_1 level as being also a valence-band state. This is in sharp conflict with the view taken up by effective-mass methods (and indeed by most classical textbooks): The latter have successfully and correctly described donor gap levels exclusively in terms of conduction-band states (cf. Sec. VI). (ii) The defect-molecule model predicts that as the binding energy of the impurity atomic *s* orbital increases, so does the binding energy of the donor gap level (measured from E_c). This is so because as the energy separation between the fixed vacancy a_1 level and the impurity *s* level increases (i.e., in going from S to O; cf. Table I), the repulsion between these two levels decreases. This is in sharp conflict with the results of the present calculation.

We conclude, therefore, that the application of the defect model to donors is incorrect. Both the hyperdeep and the gap states should be described by a single complete set of basic functions (e.g., all unper-

turbed host states) and not by an overcomplete set (e.g., a combination of pure host and impurity-atom orbitals). The binding energies of these levels hence reflect the degree of attractiveness of the screened donor potential in that part of space where the defect wave function is concentrated: A strongly attractive donor potential [e.g., Si:S in Fig. 4(b)] leads to a deeper gap level, whereas a weaker donor potential [Si:O, Fig. 4(b)] leads to a shallower donor energy. The atomic energies of the impurity need not dictate the binding energies in the solid: They merely reflect one component of the donor potential (the pseudopotential). A mathematical way of stating the invalidity of the defect-molecule model for donors rests on an overcompleteness argument. All states of the perturbed system can be described by a complete function set, e.g., the unperturbed host crystal states. Adding to this, the impurity atomic orbitals merely introduced a linearly dependent set, which may lead to erroneous conclusions.

We have been recently notified (G. DeLeo, private communication) that preliminary cluster calculations for substitutional O and S in Si show that the O a_1 level is indeed shallower than the S a_1 level by 0.37 eV [using the modified neglect of differential overlap (MNDO) approach] and by 0.32 eV (using the MS $X\alpha$ approach), in good agreement with our present results, but in contradiction to all other previous studies (Table II).

V. COMPARISON WITH EXPERIMENTS

Recently, very accurate optical excitation experiments were carried out to determine the fine structure of Se in Si.[9,10] In order to make a comparison with them we have performed transition-state calculations for both S and Se to evaluate the excitation energies between the deep a_1 level and the shallow e and t_2 gap levels. To do this we populated the a_1 level in the gap by 1.5 e and the t_2 level (also in the gap but above a_1) by 0.5 e, and carried the calculations through to self-consistency. The results are displayed in Fig. 8.

In the case of Se, the agreement with experiment is very good. Until recently, the experiments could not distinguish between $1s(e)$ and $1s(t_2)$ levels.[9,10,48] In our calculation they are 11 meV apart. In a recent work [Ref. 5(b)], the energy of the e and t_2 states of Si:Se were determined as $E_c-0.031$ and $E_c-0.034$ eV, which compares well with our results (Fig. 8) of $E_c-0.035$ and $E_c-0.046$ eV, respectively. Furthermore, there is no level of t_1 symmetry in the gap, in our calculations. Such a level is about 0.5 eV above the conduction-band minimum and highly delocalized. This is in conformity with optical experiments that report a $1s(a_1)$-$1s(t_2)$ transition, but not a $1s(a_1)$-$nl(t_1)$ transition. Finally, the Se excitation energies are 5—10% smaller than

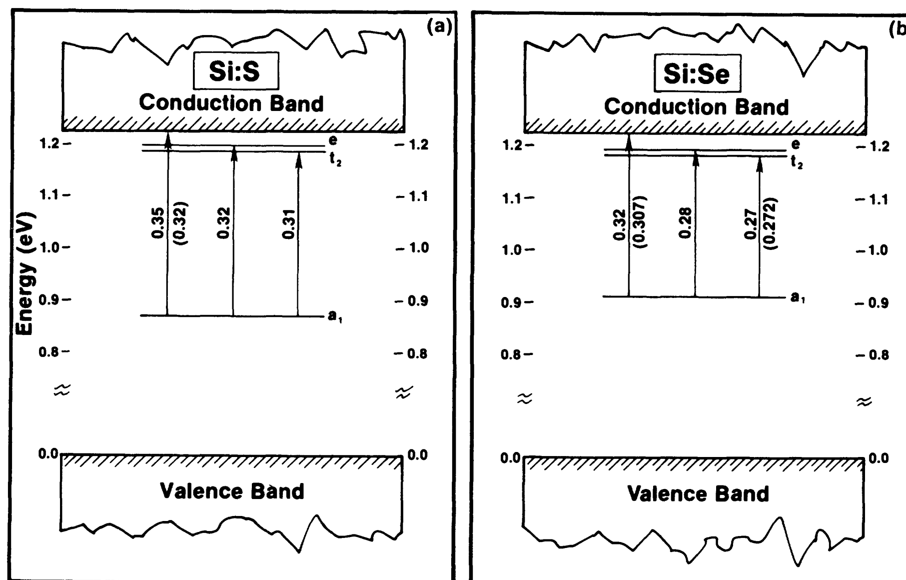

FIG. 8. Results for the transition state calculation for (a) S and (b) Se in Si. The a_1 gap level was occupied by 1.5 e and the t_2 level (also in the gap), by 0.5 e and the calculations were carried through to self-consistency.

those of S, and this again agrees with experiment.[30]

In the case of S, similar fine-structure studies have not been done until very recently.[5(b)] In a recent report by Janzén *et al.*,[5(b)] the energies of the e and t_2 levels of Si:S were determined as $E_c - 0.031$ and $E_c - 0.035$ eV. This compares well with our calculation, predicting (i.e., before the data was available) $E_c - 0.032$ and $E_c - 0.038$ eV, respectively. Humphreys *et al.*[26] have recently performed photoconductivity studies to determine the binding energies of the $1s(a_1)$, $1s(t_2)$, and the $1s(e)$ levels. They obtain 0.3184, 0.0351, and 0.0316 eV for the above-mentioned $1s(a_1)$, $1s(t_2)$, and $1s(e)$ transitions. Although a precise comparison is not possible (experiment is far more precise than theory), these experimental numbers are similar to the values given in Fig. 8(a). Further, the $1s(e)$ level lies above the $1s(t_2)$ level both in theory and experiment.

For the case of O, infrared-absorption measurements show numerous electronic transitions in the ranges 37.2–72 and 86.8–136.4 meV.[1,49] Explanations based on H and He-like donors have been attempted.[41] Phenomenological explanations based on a plausible microscopic model and using electronegativity considerations have been successful.[50] On account of the fact that our Green's-function scheme is not equipped to handle complexes, we are not in a position to make a comparison with experiment.

VI. ANALYSIS OF EFFECTIVE-MASS CALCULATIONS

Several calculations based on EMT have been reported for S and Se. Of these, those by Pantelides and Sah[37] and by Altarelli[51] seem to be the most successful. In addition, in interpreting their optical excitation and photoconductivity experiments,[9,10,25,26] the experimental workers have used effective-mass theory.[51–53] In particular, the work of Faulkner,[53] based on the point-charge model, has been used extensively. In a recent work, Jantsch *et al.*[54] have argued against the application of the EMT approach for the a_1 states. Their DLTS work shows a much stronger pressure dependence of the S and Se gap levels than what one would expect from EMT.

Our Green's-function calculation can shed light on the applicability of the EMT approach for S and Se. The impurity wave function may be expanded in terms of the host crystal Bloch states $\phi_m(\vec{k},\vec{r})$, where m is the band index and $\vec{k}$ is the Brillouin-zone wave vector[19]

$$\psi_i(\vec{r}) = \sum_m \sum_{\vec{k}} A_{im}(\vec{k})\phi_m(\vec{k},\vec{r}) . \quad (4)$$

The effective-mass calculations for donors in Si employ a single $\vec{k}$ point in the irreducible $\frac{1}{48}$ of the Brillouin zone, and one band, namely the bottom of

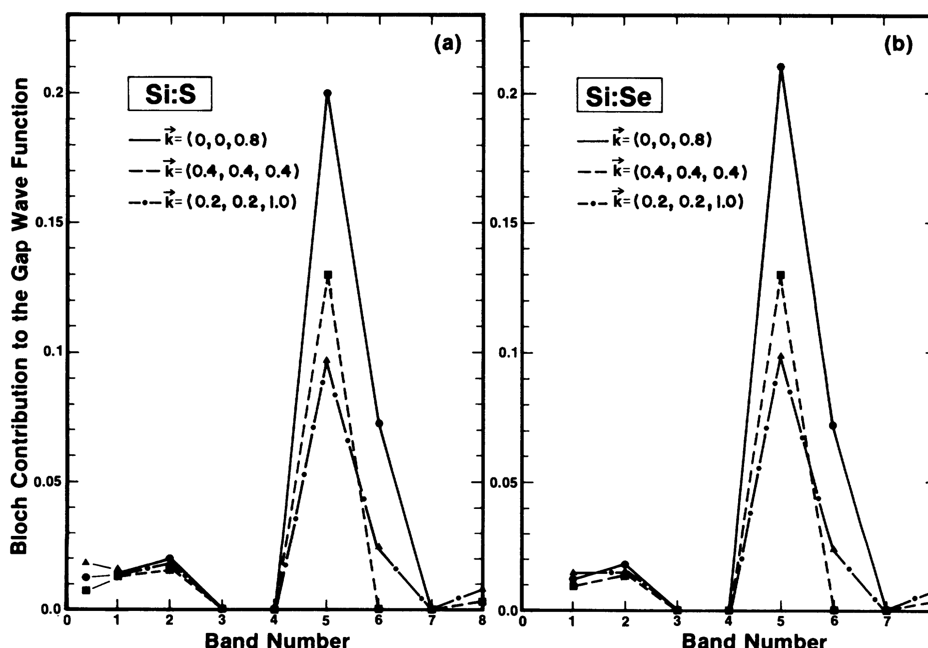

FIG. 9. Spectral decomposition of the gap a_1 wave functions of (a) Si:S and (b) Si:Se in terms of the host crystal Bloch functions [Eq. (4)].

the conduction band near point X. For this to be correct, the expansion coefficient in the general equation (4) should yield $|A_{im}(\vec{k})|^2 \simeq 1$ for this $\vec{k}$ point, i.e., $\vec{k} \simeq (2\pi/a)(0,0,0.8)$. We find (Fig. 9) that the bottom of the conduction band indeed contributes approximately 25% to the impurity gap wave function of S and Se, i.e., for $m=5$, we find

$$|A_{im}(\vec{k}=(2\pi/a)(0,0,0.8))|^2 \simeq 0.25 .$$

However, we find that there are two other points in the lowest conduction band, namely $\vec{k}=(2\pi/a)(0.4,0.4,0.4)$ and $\vec{k}=(2\pi/a)(0.2,0.2,1)$ with significant contributions (13% and 12%, respectively) to this a_1 gap wave function. Thus the lowest conduction band contributes approximately 50%. The lowest valence band contributes about 5% to this a_1 gap state. The remaining 45% is mostly contributed by higher conduction bands throughout the Brillouin zone. This reveals the multiband character of the a_1 gap state and casts some doubt on the EMT calculations for the ground-state binding energy. The conclusions based on Fig. 9 do not apply to excited states or to very shallow states. These could very likely be effective-mass-like. Indeed, Humphreys *et al.*[26] have found that the binding energy for the excited p states of S is in good agreement with effective-mass theory.

ACKNOWLEDGMENTS

We gratefully acknowledge useful discussion and correspondence with P. Bendt, J. W. Corbett, G. DeLeo, E. Janzén, G. Oehrlein, S. N. Sahu, B. Skarstam, J. Swartz, and R. Thurber. Special thanks are due E. Janzén for communicating to us his recent results on the e and t_2 gap levels of Si:S and Si:Se [Ref. 5(b)] after this work was completed, and for helpful critical comments on the manuscript. We thank the staff of the Solar Energy Research Institute (SERI) computer center for their assistance. One of the authors (V.A.S.) acknowledges support from SERI under Subcontract No. HS-0-9188.

*Present address: Tata Institute of Fundamental Research, Home Bhabha Road, Bombay 400005, India.

[1]G. Oehrlein, Ph.D. thesis, S.U.N.Y. Albany, 1981 (unpublished), and references therein.

[2]S. Kishino, in Proceedings of the 15th International Conference on the Physics of Semiconductors, Kyoto, Japan [J. Phys. Soc. Jpn. 49, Suppl. A (1980)].

[3]J. R. Patel, in *Semiconductor Silicon 1981,* edited by H. R. Huff, R. J. Kriegler, and Y. Takeishi (Electrochemical Society, Pennington, New Jersey, 1981).

[4]G. D. Watkins and J. W. Corbett, Phys. Rev. 121, 1001 (1961); J. W. Corbett, G. D. Watkins, R. M. Chrenko, and R. S. McDonald, *ibid.* 121, 1015 (1961).

[5](a) E. Janzén, Ph.D. thesis, University of Lund, 1981 (unpublished), and references therein; (b) E. Janzén, R. Stedman, and H. G. Grimmeiss, International Conference on the Physics of Semiconductors, Montpellier, France, 1982 (in press).

[6]S. D. Brotherton, M. J. King, and G. J. Parker, J. Appl. Phys. 52, 4649 (1981).

[7]P. Migliorato and C. T. Elliot, Solid State Electron. 21, 443 (1978).

[8]H. R. Vydyanath, W. J. Helm, J. S. Lorenzo, and S. T. Hoelke, Infrared Phys. 19, 93 (1979).

[9]J. C. Swartz, D. H. Lemmon, and R. N. Thomas, Solid State Commun. 36, 331 (1980).

[10]B. Skarstam and J. L. Lindstörm, Appl. Phys. Lett. 39, 488 (1981).

[11]C. E. Fischer, *The Hartree Fock Method for Atoms* (Wiley, New York, 1977).

[12]W. Lotz, J. Opt. Soc. Am. 60, 206 (1970).

[13]J. C. Slater, *Symmetry and Energy Bands in Crystals* (Dover, New York, 1972), p. 55.

[14]L. Pauling, *The Nature of the Chemical Bond,* 3rd ed. (Cornell University Press, Ithaca, New York, 1960), p. 246.

[15]R. T. Sanderson, *Chemical Bonds and Bond Energy,* 2nd ed. (Academic, New York, 1976), p. 41.

[16]L. Pauling, Ref. 14, p. 93.

[17]V. A. Singh and A. Zunger, Phys. Rev. B 25, 907 (1982).

[18]F. A. Trumbore, Bell Syst. Tech. J. 3 39, 705 (1960).

[19]U. Lindefeldt and A. Zunger, Phys. Rev. B 24, 5913 (1981); 26, 846 (1982).

[20]A. Zunger and M. L. Cohen, Phys. Rev. B 18, 5449 (1978); 20, 4082 (1979).

[21]E. Fuess, Ann. Phys. (Leipzig) 80, 367 (1926); V. A. Singh, U. Lindefelt, and A. Zunger, Bull. Am. Phys. Soc. 27, 278 (1982).

[22]A. Zunger and U. Lindefelt, Phys. Rev. B 27, 1191 (1983).

[23]H. G. Grimmeiss, E. Janzén, and B. Skarstam, J. Appl. Phys. 51, 4212 (1980).

[24]H. G. Grimmeiss, E. Janzén, and B. Skarstam, J. Appl. Phys. 51, 3740 (1980); 51, 6238 (1980).

[25]H. G. Grimmeiss, E. Janzén, and K. Larsson, Phys. Rev. B 25, 2627 (1982).

[26]R. G. Humphreys, P. Migliorato, and G. Furtunato, Solid State Commun. 40, 819 (1981).

[27]D. R. Myers and W. E. Phillips, Appl. Phys. Lett. 32, 756 (1978).

[28]G. W. Ludwig, Phys. Rev. 137, A1520 (1965). Ludwig's attempt to relate the resonance signal to a definite energy position in the gap is based on the work of

Kravitz [L. C. Kravitz, Ph.D. thesis, Harvard Universiy, 1965 (unpublished)], who found a marked decrease in the resonance signal for photon energies ≥ 0.59 eV. The identification with S II (*D* level) is thus very plausible.

[29]W. E. Krag, W. H. Kleiner, H. G. Zeiger, and S. Fischler, J. Phys. Soc. Jpn. 21, 230 (1966).

[30]H. G. Grimmeiss and B. Skarstam, Phys. Rev. B 23, 1947 (1981).

[31]Saar Muller, Ph.D. thesis, Amsterdam University, 1981 (unpublished); S. H. Muller, M. Sprenger, E. G. Sieverts, and C. A. J. Amerlaan, Solid State Commun. 25, 987 (1978).

[32]J. W. Chen and A. J. Milnes, Annu. Rev. Mater. Sci. 10, 157 (1980).

[33]M. Yokoi, T. Nomura, and K. Yamasaki, J. Am. Chem. Soc. 77, 4484 (1955).

[34]C. T. Prewitt and H. S. Young, Science 149, 535 (1965).

[35]N. H. Fletcher, Ph.D. thesis, Harvard University, 1955 (unpublished). To our knowledge, this was the first time a defect Green's-function approach was employed to perform detailed calculations for defects in semiconductors. See also L. M. Roth, Ph.D. thesis, Harvard University, 1957 (unpublished).

[36]H. P. Hjalmarson, P. Vogl, D. J. Wolford, and J. D. Dow, Phys. Rev. Lett. 44, 810 (1980); H. P. Hjalmason, Ph.D. thesis, University of Illinois at Urbana-Champaign, 1979 (unpublished); P. Vogl, in *Festkörperprobleme,* edited by J. Treusch (Vieweg, Braunschweig, 1981); Vol. 21, p. 191.

[37]S. T. Pantelides and C. T. Sah, Phys. Rev. B 10, 621 (1974); 10, 638 (1974).

[38]S. T. Pantelides, in *Festkörprobleme,* edited by H. J. Queisser (Pergamon-Vieweg, Braunschweig, 1975), Vol. XV, p. 149.

[39]J. Bernholc, N. O. Lipari, S. T. Pantelides, and M. Scheffler, in *Proceedings of the International Conference on Defects in Semiconductors, Oisio, Japan, 1980,* edited by R. R. Hasiguti (IOP, London, 1981), p. 1.

[40]T. H. Ning and C. T. Sah, Phys. Rev. B 4, 3468 (1971); 4, 3482 (1971).

[41]A. Glodeanu, Phys. Status Solidi 19, K43 (1967).

[42]S. T. Pantelides, Rev. Mod. Phys. 50, 797 (1978).

[43]B. G. Cartling, J. Phys. C 8, 3183 (1975).

[44]M. J. Caldas, J. R. Leite, and A. Fazzio, Phys. Status Solidi B 98, K109 (1980).

[45]J. E. Huheey, *Inorganic Chemistry* (Harper and Row, New York, 1977), p. 605.

[46]J. C. Phillips, Phys. Rev. Lett. 24, 1114 (1970); Phys. Rev. B 1, 1540 (1970); 1, 1545 (1970).

[47]G. A. Baraff, E. O. Kane, and M. Schlüter, Phys. Rev. B 25, 548 (1982).

[48]J. C. Swartz (private communication); B. Skarstam (private communication).

[49]D. Wruck and P. Gaworzewski, Phys. Status Solidi B 56, 556 (1979).

[50]S. N. Sahu, Tian-sheng Shi, Pei-wan Ge, A. Hiraki, T. Imura, M. Tashiro, V. A. Singh, and J. W. Corbett, J. Chem. Phys. (in press); T. S. Shi, S. N. Sahu, G. S. Oehrlein, A. Hiraki, and J. W. Corbett, Phys. Status Solidi (in press).

[51]M. Altarelli, W. Y. Hsu, and R. A. Sabitini, J. Phys. C 10, L605 (1977); M. Altarelli (unpublished).

[52]L. M. Roth, MIT Lincoln Laboratory Solid State Research Report No. 3 (unpublished).

[53]R. A. Faulkner, Phys. Rev. 184, 713 (1969).

[54]W. Jantsch, K. Wunstel, O. Kumagai, and P. Vogl, Phys. Rev. B 25, 5515 (1982).